# MECHANICAL PROPERTIES OF C-S-H GLOBULES AND INTERFACES BY MOLECULAR DYNAMICS SIMULATION

Ding Fan[1] and Shangtong Yang[1*]

[1] *Department of Civil and Environmental Engineering, University of Strathclyde, Glasgow, G1 1XJ, United Kingdom.*

## ABSTRACT

At meso-scale, Calcium Silicate Hydrate (C-S-H) can be considered as randomly packed globules (about 4.2nm), which forms the basic unit cell, with water molecules and voids. In this paper, the nanostructures for the globules are developed based on some plausible atomic structures of C-S-H. The mechanical properties for the C-S-H globules are determined through molecular dynamics simulation. Interfaces between the C-S-H globules are also simulated with different amount of water molecules. Key material parameters, e.g., Young's modulus, strength and fracture energy, are obtained. It has been found that longer mean chain length of silicate tends to increase the strength of C-S-H and change the fracture behavior from brittle to ductile failure, in the chain length direction. In the other direction, however, silicate chains do not play an important role while interlayer structure matters. Moreover, pores in the C-S-H nanostructures can considerably reduce the strength of the globule structures in the normal direction to silicate chain but the weakening effect becomes substantially less in silicate chain direction. Further, it has been found that for all types of the interfaces between C-S-H globules, the interface with no extra water molecules has the greatest tensile/shear strength. The mechanical properties obtained in this paper for C-S-H nanostructures and interfaces are necessary inputs to the meso-scale modelling of C-S-H via either granular mechanics, i.e., DEM, or continuum mechanics, i.e., FEM.

## KEYWORDS

C-S-H; mechanical properties; molecular dynamics modeling; interfaces; colloidal model; meso-scale.

* Corresponding author. Tel: +44 141 5483273. Email: shangtong.yang@strath.ac.uk.

## 1. INTRODUCTION

Since the invention of modern cement, there has been considerable mass of research carried out in improving cement characteristics in terms of toughness [1], strength [2, 3] and durability [4, 5]. Recently, there is a growing research interest in modeling the atomic structure and investigating the nano/micro-scopic properties of cement [6-10]. In light of difficulties in conducting experimental tests at the nano/micro-scale level, atomic modeling provides a unique view in understanding the fundamental behavior, especially mechanical properties, of the cementitious materials.

Calcium Silicate Hydrates (C-S-H) gel is the main binding phase of the cement hydration products, significantly contributing to the cohesion and strength of cement. C-S-H gel is known as imperfect crystalline and a close analogue of Tobermorite and Jennite minerals. In the past three decades, a number of crystalline models for C-S-H structure were identified or developed, based on the well-known Tobermorite and/or Jennite structures [11-17]. 14 Å Tobermorite and Jennite are the most common crystalline phases presented, whereas the modelling of real imperfect crystalline structure of the C-S-H gel is tremendously challenging. Generally, the C-S-H structure can be characterized in terms of calcium/silicon (Ca/Si) ratio which normally ranges from 0.6 to 2.3 [18]. 14 Å Torbermorite has a chemical formula $Ca_5Si_6O_{16}(OH)_2 \cdot 7H_2O$ and a density of 2.18g/cm$^3$. Typical Jennite has a Ca/Si ratio of 1.5, a density of 2.27 g/cm$^3$ and a formula $Ca_9Si_6O_{18}(OH)_6 \cdot 8H_2O$ [19]. Accordingly, Richardson [14] has developed Tobermorite/Jennite (T/J) model and Tobermorite/Calcium Hydroxide (T/CH) model for C-S-H. The T/J model is a combined Tobermorite and Jennite domains while the T/CH model contains Tobermorite silicate chains sandwiching calcium hydroxide, providing higher Ca/Si ratios. Another widely-cited C-S-H model is the so-called realistic molecular structure of C-S-H, developed by Pellenq and his co-workers [20]. This model has defected silicate chains, consisting of silicate monomers, dimers and pentamers. It has a Ca/Si

ratio of 1.65 which is close to the recent experimental findings, i.e., $(CaO)_{1.7}(SiO_2)(H_2O)_{1.80}$, by neutron scattering measurements [21]. They postulated that the Ca/Si ratio remains the most important parameter in any model construction of C-S-H. Moreover, Richardson [22] developed a series of models for C-S-H with Ca/Si lower than 1.4 representing different mean chain lengths using crystal-chemical and geometrical reasoning.

Based on the C-S-H models, atomic simulation, mainly through molecular dynamics (MD) modeling, have been conducted in recent years to determine the mechanical properties of C-S-H. Al-Ostaz, et al. [23] simulated the mechanical properties of the 14 Å Tobermorite, Jennite and calcium hydroxide. They have found that the force field chosen and size of simulation box affected the results. For example, different force fields resulted in different mechanical properties. Moreover, the C-S-H unit needed to be duplicated 3×3×3 to match the experimental mechanical properties for initial MD modeling as the mechanical properties of the original unit and 2×2×2 supercell were not very close to the experimental data. Moreover, Hou, et al. [24] modeled the C-S-H structure based on the 11Å Tobermorite [25] with ClayFF force field [26] and investigated the effects of the water layer, silicate chain, and Calcium atoms in the interlayer on the mechanical properties of C-S-H. Other than elastic properties, MD simulation can also be employed to study the fracture properties of cement at the nanoscale. A similar structure as proposed in Pellenq, et al. [20] was used and duplicated several times to form a cube with the size of 13.8 nm; direct tension was then applied to investigate the Mode I fracture of C-S-H under CSHFF force field [27]. It has been found that Ca-O and Si-O bonds were provided to contribute the most cohesive force on xy plane, and weaker H- bonds bind the structure on z plane. In addition, size effects have been shown as result of different size of the central voids made by deleting different number of atoms, on weakening stiffness and cohesive force of C-S-H. Further, fracture toughness of C-S-H were

evaluated by MD simulations, and the brittleness was discussed in comparison with other brittle materials at the atomic scale [28].

When the structure of C-S-H evolves from nanoscale to mesoscale, it is much more unclear. There are perhaps only two widely acknowledged models, namely, Colloidal model [29, 30] and Feldman-Sereda model [31], to describe the mesostructure of C-S-H. In Jenning's Colloidal model, a globule (about 4.2nm) forms the basic unit cell which is a discrete nano particle; the globules are not linked together but packed randomly with water molecules and voids. In Feldman-Sereda model, however, long layers of C-S-H are well aligned and extend from one nanocrystalline region to another. The 4.2nm unit cell (globule) of C-S-H in the Colloidal model has four or five layers of silicate chains, sandwiching Calcium ions, water molecules and possibly pores. The unit cell then discretely joins each other in different directions to form the mesostructure of C-S-H. To simulate the mesoscale mechanical properties of C-S-H, granular mechanics would be of much interest; however, the mechanical properties of the globule itself and the interfaces on the joining surfaces of these nanostructure cells would need to be obtained in advance. This paper attempts to determine the basic mechanical properties of the globule of C-S-H and the interfaces of the globules in terms of different water contents. The atomic structure of C-S-H in Richardson [14] and the ReaxFF force field are employed in the molecular dynamics simulation. The results in this study will provide important and necessary input for mesoscale modeling of C-S-H by either discrete element modeling or finite element modeling.

## 2. MODEL CONSTRUCTION

The atomic structures of C-S-H used in this paper are chosen from Richardson [22], i.e., T2_ac and T11_14sc. T2_ac is a double-chain Tobermorite-based monoclinic structure, derived from Merlino, et al. [32] in which all the interlayer Ca atoms are in octahedral coordination with oxygen atoms in silicate chains, as shown in Figure 1(a). T11_14sc is also a Tobermorite-based monoclinic structure but the mean length of

silicate chains is 11 Å and the layer spacing is 14 Å, as presented in Figure 1(c). Based on these two structures, two orthorhombic structures are generated (Figure 1(b) and (d)). Moreover, in Jennings's Colloidal model intragobular pores (IGP) may exist in the unit cell of globule and the effects of IGP have not been addressed or simulated yet. In this paper, a structure containing IGP is produced as shown in Figure 1(e). And the characteristics of all five models is listed in Table 1. All structures are tested under uniaxial tension along y and z axis. For T2_ac molecular structure with chemical formula $Ca_4H_2(Si_2O_7)_2Ca_4H_20$, the lattice parameters of a = 11.35 Å, b = 7.3 Å, c = 21.5 Å and β = 98.4° with space group C12/c1 are duplicated as 4 × 6 × 2 along x-, y-, z- directions, respectively, to generate Model I; the structure is then changed to orthorhombic structure, where the volume, density, atom position and bonds information are kept the same, as named Model II. For T11_14sc molecular structure with chemical formula $Ca_9(Si_{11}O_{28}(OH)_6)(H2O)_{7.25}$, the lattice parameters of a = 11.35 Å, b = 7.3 Å, c = 52.7 Å and β = 95.5° with space group C1 are duplicated as 4 × 6 × 1 supercell along x-, y-, z- directions, respectively, to generate Model III; the structure is then changed to orthorhombic, namely, Model IV. Model V is the IGP structure. LAMMPS [33] is used to perform the MD simulations.

Model III and Model IV have advantages to be used as the basic structure to investigate the effects of IGP [30] on the mechanical properties of C-S-H, since the interlayer Calcium atoms have the occupancy lower than 1.0 which can be arranged in MD simulation for a targeting structure. In this paper, Model IV is modified by rearranging the first upper interlayer Calcium atoms in the unit with a number of water molecules to maintain appropriate Ca-O coordination number [22], for a porosity of 10.43%, shown as Model V in Figure 1(e). All simulation boxes, i.e., Models I – V, are relaxed for 50 ps in the isobaric-isothermal ensemble (NPT) and coupled to zero external pressure in the x, y, z dimensions. The Nose-Hoover thermostat is used to keep the temperature at 300 K, and the Nose-Hoover barostat is

used to maintain the pressure at p = 0Pa. After it reaches equilibrium, the system is subjected to the tensile load along y- and z-direction with a constant strain rate at 0.08 Å/ps. For the strain-stress relation along y direction, the pressures in the x and z directions are kept at zero, and for the strain-stress relation along z direction, the pressures in the x and y directions are kept at zero.

ReaxFF has been extensively used in simulating the molecular behavior of C-S-H structures, e.g., [34, 35]. In general, ReaxFF can simulate the chemical and physical interactions between Ca, Si, O, H atoms in the C-S-H gel and the interfaces. The potential energy defined by the ReaxFF can be expressed as follows [36]:

$$E_{system} = E_{bond} + E_{lp} + E_{over} + E_{under} + E_{val} + E_{pen} + E_{coa} + E_{C2} + E_{tors} + E_{conj} + E_{H-bond} + E_{vdWaals} + E_{Coulomb} \quad (1)$$

where $E_{bond}$ is bond energy, $E_{lp}$ is long pair energy, $E_{over}$ is over coordination energy, $E_{under}$ is under coordination energy, $E_{val}$ is valence angle energy, $E_{pen}$ is penalty energy, $E_{coa}$ is three-body conjugation energy, $E_{C2}$ is C=C correction, $E_{tors}$ is torsion rotation energy, $E_{conj}$ is four-body conjugation energy, $E_{H\text{-}bond}$ is hydrogen bond interaction energy, $E_{vdWaals}$ is van der Waals interaction energy and $E_{Coulomb}$ is coulomb interaction energy. The energy of per atom is calculated by defined potentials from neighbor atoms. In the present study, not all of terms in Eq.(1) are considered necessary and some of them are set to zero, which reduces terms of the energy expression as follows:

$$E_{\mathrm{system}} = E_{bond} + E_{over} + E_{val} + E_{tors} + E_{vdWalls} + E_{Coulomb} \quad (2)$$

***Interfaces between the globules***

Jennings's Colloidal model (2008) sheds light on simulating the mesoscale mechanical properties of C-S-H by using granular mechanics, i.e., discrete element method, or continuum mechanics, i.e., finite element method. No matter which

method is used to simulate the meso system of C-S-H, the interfacial properties between the unit globules should be known as a prior. To investigate the normal and shear strengths at the interfaces in different directions, two supercells of Model IV are connected to each other along (100), (010) and (001) planes. Five different thicknesses of water layers are added in the interface to investigate the effect of water content on the interfacial properties, 0.0, 0.5, 1.0, 1.5, 2.0 Å, respectively. The density for water is 1 g/cm$^3$ and the Water/Si ratio for each model is 0.66, 0.86, 1.04, 1.25 and 1.37, respectively. The simulation box is relaxed for 50 ps in the isobaric-isothermal ensemble (NPT) and coupled to zero external pressure in the x, y, z dimensions. After that, the boundaries are changed to non-periodic and shrink-wrapped in three dimensions for the shear test and the microcanonical ensemble (NVE) is employed. During each shear test, the bottom atoms are fixed and the top atoms are loaded to move along the interface with a constant loading rate at 0.08 Å/ps. During each tensile test, the bottom is fixed and the top is moved vertically to the interface with a constant loading rate of 0.08 Å/ps.

## 3. RESULTS AND DISCUSSION

### 3.1 Mechanical properties for C-S-H globules

The complete tensile test simulations for the C-S-H globules along y- and z-directions (along silicate chains and normal to silicate chains respectively) are shown in Figure 2. In addition, the direct tensile stress-strain relationships obtained are shown in Figure 3. In y-direction, all the five structures present linear increases in the initial elastic stage while Model I and II have slightly lower elastic modulus than the other three structures. Model I and II have very close tensile stress-strain relationship which has the maximum stress about 9 GPa at the strain of 0.11. These two structures are very brittle, since following the maximum value, the stress suddenly reduces to 4.5 GPa and keeps constant for the next 0.2 straining. It then gradually decreases until the complete separation. For Models III, IV and V, the stresses develop in similar

trend and increase up to about 11 GPa. Different from Model I and II, these three structures undergo a clear ductile development before they gradually decrease. Such a ductile stage in the mechanical behavior is caused by the longer mean length of the silica chains, which provide higher force carrying capability during tensile test along the y-direction. Moreover, it is interesting to find that the Model V (i.e., IGP structure) has some minor strength decrease at y-direction, compared with Models 3 and 4. This means the intralayer pores can slightly affect the mechanical properties in the silicate chain length direction. It makes sense as the y-direction mechanism is mainly provided by the silicate chains which are not significantly affected by these pores. In z-direction which is the direction vertical to the silica chain, Models I and II have much higher strengths compared with Models III, IV and V. The stress-strain curves for Models I and II in z-direction are close to those in y-direction except for the softening pattern. However, the C-S-H structures of Models III – V have much lower strengths in z-direction in comparison with those in y-direction. This is because the interlayer Calcium and water interface in Models III – V provide a weaker connection compared to Model I and II, where the Calcium atom is in octahedral coordination with oxygen atoms resulting in much stronger interactions. Compared to Models III and IV, Model V (IGP structure) has much lower strength, i.e, 1.15GPa, while the Model III and IV go up to 1.9 GPa. It demonstrates that the existence of IGP can significantly reduce the strength of the C-S-H globules in the z-direction (i.e., the normal direction to the silicate chains).

The modulus of Elasticity calculated from the stress-strain curves and the maximum stress of each structure of C-S-H are shown in Table 2. The Young's modulus of the five structures along z-direction is in the range of 39 GPa to 54 GPa, which is reasonable compared to the experimental data of cements in range of 38 GPa to 56 GPa for wetted cement with low porosity and simulation data of tobermorite-like and jennite-like structures in range of 35 GPa to 56 GPa [37, 38]. The strength of each

structure is also in the reasonable range compared to tobermorite-like structure at about 1.4 GPa along z-direction and 9 GPa along y-direction [28, 39]. The Young's modulus in y direction increases when the C-S-H gel changes to orthorhombic from monoclinic. By contrast, the strengths in y and z directions and the Young's modulus in z direction reduce for the orthorhombic structure. The change of crystal system has an impact on the mechanical properties; although the difference is not significantly large, it needs to be rigorous in establishing C-S-H structures. On the other hand, for some large scale molecular system modelling or interfacial properties study, the structure will need to be changed slightly under duplication or packing or fitting in simulation box. Interestingly, Model V shows lower mechanical capacity, especially in z-direction, with 28% and 40% reduction for modulus of Elasticity and strength compared to Model III, respectively. Under loading the existence of IGP will cause rearrangement of Calcium in the interlayer.

### 3.2 Mechanical properties for the interfaces between C-S-H globules

Figure 4 illustrates Model IV packed with 0 to 2 Å water layer interface on different surfaces of the globules, and the structure with W0, W5, W10, W15, W20 stand for the interface with a water layer of 0.0, 0.5, 1.0, 1.5, 2.0 Å added, respectively. The force $F_i$ exerted on atom $i$ is given by $F_i = -\frac{\partial E_i}{\partial r_i}$, where $E_i$ is the interaction energy for atom $i$, and $r_i$ is the position of atom $i$. The total shear force $F$ on the fixed atoms is calculated by $F = \sum F_i$. The tensile force $F$ is considered as being transferred to the interface between two C-S-H globules. The stress at the interface can be calculated as follows:

$$\sigma = \frac{F}{A} \tag{3}$$

where $F$ is tensile force at the interface, and $A$ is the force-resisting area. Due to the tensile test, the area in Equation (3) is kept constant, the tendency of the

force-displacement and stress-strain curve is the same and only the stress-strain curves are shown in Figure 5.

For all three types of interfaces, the interface with no extra water molecules has greatest tensile strength compared to other structures with added water, because of the destructive effect of water on the bond generation between two C-S-H globules. For (001) interface, the stresses of other four structures with different amount of water molecules added present similar properties and there is no significant difference among the maximum value of stress, initial elastic stage and trend of curve. For (010) and (100) interfaces, the slope of initial elastic stage and the maximum value of stress both decrease with the increase of water content. The details of the tensile mechanical properties calculated from Figure 5 are shown in Table 3.

Young's modulus is defined by the slope of the initial elastic stage. Compared to the mechanism analysis of C-S-H globules during compressing test, the results in this study cover different Young's modulus between C-S-H interfaces in range of 10 GPa to 37 GPa in three elastic stage under compression [40]. The fracture energy $G_F$ is determined from the area under the stress-strain curves in Figure 5, multiplied by the initial length of the simulation box. For (001) surface, with water molecules added, the maximum stress, Young's modulus and fracture energy show no significant difference among different water content. For (010) and (100) surfaces, the maximum stress and Young's modulus decrease with the increase of water molecules. The minimum values of the fracture energy in three interface types all show in the structure with 2.0 Å and 1.5 Å water layer. It is interesting that the maximum value of stress and Young's modulus of W0 structure in (010) interface are almost the same as the value of Model III along y-direction in Table 2. This is because Reaxff allows bond breakage and generation so that the interface reconnects as one C-S-H unit during equilibrium to form the original structure. For further simulation such as FEM

and DEM, the results in (001) interface are recommended, because it is the natural cleavage plane which is also the weakest layer in the C-S-H structure [41]. The tensile properties are calculated by the average of four structures with extra water molecules as: $\sigma_{max} = 0.98 \pm 0.09$ Gpa ; Young's modulus $E = 29.92 \pm 3.55$ GPa ; Fracture energy $G_F = 0.47 \pm 0.13\ J/m^2$.

The shear properties for the interfaces of C-S-H globules with different water content are also simulated and the shear force – displacement curves are shown in Figure 6. The shear force $F$ is directly related to the interfacial stress transfer and can be used as the basis to derive the interfacial shear strength of the globule interfaces. Figures 6(a)-(c) show the relation between the shear force along moving direction *F* and the shear displacement for different thickness of water layers for the three types of interfaces. For 001 surface, all the five curves start to increase linearly. The maximum force is achieved for the water layer 0 Å, which is 313.4 $kcalmol^{-1}Å^{-1}$ at 5.4 Å shear displacement. After the maximum value of each curve, the shear force along x direction gradually decreases with fluctuation. It can be found that the effect of water layer is significant for 001 surface since the overall shear force of 0 Å water layer is much higher than that of the other four interfaces. This indicates that the water molecules interdict the intralayer Calcium-Oxygen bonding between the globules. The shear force fluctuates over the displacement which is normal for molecular dynamics simulation.

According to Amonton's law of adhesion [42], the friction force F is divided into two parts*:* $F = \mu L + F_0$, the external normal force L multiplied by the friction coefficient $\mu$ and the internal force $F_0$ impacted by the adhesion between the surface. In this study, $L$ continuously decreases due to the reduction of the contact surface in the globules interface; the internal force $F_0$ should initially increase because of bond stretching and then decrease due to bond breakage. During any fluctuation stage of *F*,

the generation and breakage of bonds in the interface both happen. The shear force–displacement generally follows Amonton's law for individual curves. The simulation of the interfacial shearing clearly shows both the chemical interaction (i.e. bonding) and the physical interaction occurring at the interface between two globules for three surfaces, as shown in Figure 4. The shear stress $\tau$ can be determined as follows:

$$\tau = \frac{F}{A_{CSH-CSH}} = \frac{F}{a_0 \times (b_0 - \Delta b)} \quad (4)$$

where $A_{CSH\text{-}CSH}$ is the contact area between two C-S-H globules in the interface, $a_0$ is the length of C-S-H vertical to the shear direction, $b_0$ is the width of C-S-H along the shear direction and $\Delta b$ is the shear distance of the moving C-S-H globule. For (001) surface, $a_0 = 43.43$ Å , $b_0 = 50.60$ Å, for (010) surface, $a_0 = 41.60$ Å , $b_0 = 32.43$ Å, and for (100) surface, $a_0 = 50.60$ Å, $b_0 = 41.60$ Å, respectively. By using Eq. (4) and the values of $a_0$ and $b_0$ above, the shear stress can be calculated as a function of the displacement for each surface. Figures 7 (a), (c) and (e) show the relationship between the shear stress and displacement and Figures 7 (b) (d) and (f) present the maximum shear stress, average shear stress and error bars. The average stress is calculated after the first peak stress. In the shear stress-strain curves for all three interfaces, stresses all increase first and then fluctuate over certain values. Such a shearing mechanism of the interfaces can be simplified to a linear increase, followed by a constant development over the strain; or it may be called bi-linear stress-strain curves which can be easily implemented in FEM or DEM modelling. This yielding-like shearing behaviour after its peak stress is not commonly seen in macroscale shear stress development in cementitious materials, where the shear stress usually drops after its strength. It can be found out that the shear strength, i.e., the maximum shear stress, for any type of interfaces of the C-S-H globules, has the highest value when no water layer exists. When water molecules are presented at the interfaces, however, the strength is reduced. Another interesting finding is the content of water molecules is not a very sensitive parameter. For example, the average stresses for W5, 10, 15 and 20 of all these interfaces are relatively the same, as shown

in Figures 7 (b), (d) and (f). The interfacial shear strength of C-S-H globules interface is then calculated by the average value of the stress for (001) surface with 0.5 Å, 1.0 Å, 1.5 Å and 2.0 Å water layer thickness to be about 560.29 ± 135.44 MPa; for (010) surface is about 780.63 ± 39.51 MPa; and for (100) surface, the shear strength is about 564.53 ± 78.33 MPa.

The shear stress-displacement curves, often known as bond-slip relation, for the C-S-H globule interfaces and the mechanical properties for C-S-H globules are derived for C-S-H. These properties have been hardly seen in existing literature. It has significant impact on multi-scale modeling (either FEM or DEM) in terms of providing necessary inputs for the nanoscale C-S-H structures. These properties are usually not available due to difficulties in conducting experiments. This is why trial and error analysis is always applied for estimating the mechanical properties. The mechanical properties derived in this paper can well be used for defining the bond-slip behavior between the unit C-S-H globules as well as the constitutive relation for the globule itself.

## 4. CONCLUSIONS

In this paper, the C-S-H globules and the interfaces between the C-S-H globules have been modeled at the atomic scale and the complete mechanism has been studied through MD simulations. Reaxff was used to provide the interactive potentials for the whole molecular system. Key material parameters, e.g., Young's modulus, strength and fracture energy, were determined for the globules and interfaces. It has been found that the atomic structure significantly affects the mechanical performance of the C-S-H structures. Longer mean chain lengths (i.e., Models III - V) tend to increase the strength of C-S-H and, more importantly, change the fracture behavior from brittle failure to ductile failure, along the silicate chains direction. In the direction normal to silicate chains, however, silicate chains do not play an important role while interlayer

structure matters. Octahedral coordination of Calcium with oxygen atoms will result in stronger interactions and higher mechanical strengths in the normal direction. Moreover, pores (i.e., IGP) in the C-S-H globules can considerably reduce the strength of the globule structures in normal to silicate chain direction but the weakening effect becomes less significant in silicate chain direction. Further, the effects of water content at the interfaces between globules were investigated and the normal strength and the shear strength for the interfaces were determined. It has been found that, for all types of the interfaces, the interface with no extra water molecules has greatest tensile/shear strength, because of the destructive effect of water on the bond generation between two C-S-H globules. However, it is interesting to find the strength is not very sensitive to the amount of water since different water content at the interfaces resulted in roughly similar mechanical performance. It can be concluded that the mechanical properties obtained in this paper for C-S-H nanostructures and interfaces are highly complementary to the meso-scale modelling of C-S-H via granular mechanics, i.e., DEM, or continuum mechanics, i.e., FEM.

## ACKNOWLEDGMENTS

Partial financial support from the European Commission Horizon 2020 Marie Sklodowska-Curie Research and Innovation Staff Exchange scheme through the grant 645696 (i.e. REMINE project) is greatly acknowledged.

## REFERENCES


[1] K. Sobhan and M. Mashnad, "Tensile strength and toughness of soil–cement–fly-ash composite reinforced with recycled high-density polyethylene strips," *Journal of Materials in Civil Engineering*, vol. 14, no. 2, pp. 177-184, 2002.

[2] M. Ali, A. Majumdar, and D. Rayment, "Carbon fibre reinforcement of cement," *Cement and Concrete Research*, vol. 2, no. 2, pp. 201-212, 1972.

[3] W. Sonphuak and N. Rojanarowan, "Strength improvement of fibre cement product," *International Journal of Industrial Engineering Computations*, vol. 4, no. 4, pp. 505-516, 2013.

[4] J. Claramunt, M. Ardanuy, J. A. García-Hortal, and R. D. Tolêdo Filho, "The hornification of vegetable fibers to improve the durability of cement mortar composites," *Cement and Concrete Composites*, vol. 33, no. 5, pp. 586-595, 2011.

[5] S. Leonard and A. Bentur, "Improvement of the durability of glass fiber reinforced cement using blended cement matrix," *Cement and concrete research*, vol. 14, no. 5, pp. 717-728, 1984.

[6] O. Bernard, F.-J. Ulm, and E. Lemarchand, "A multiscale micromechanics-hydration model for the early-age elastic properties of cement-based materials," *Cement and Concrete Research*, vol. 33, no. 9, pp. 1293-1309, 2003.

[7] L. Feng and M. Christian, "Micromechanics model for the effective elastic properties of hardened cement pastes," *Acta Materiae Compositae Sinica*, vol. 24, no. 2, pp. 184-189, 2007.

[8] C.-J. Haecker *et al.*, "Modeling the linear elastic properties of Portland cement paste," *Cement and Concrete Research*, vol. 35, no. 10, pp. 1948-1960, 2005.

[9] F.-J. Ulm, G. Constantinides, and F. Heukamp, "Is concrete a poromechanics materials?—A multiscale investigation of poroelastic properties," *Materials and structures*, vol. 37, no. 1, pp. 43-58, 2004.

[10] W. Wu, A. Al-Ostaz, A. H.-D. Cheng, and C. R. Song, "Concrete as a hierarchical structural composite material," *International Journal for Multiscale Computational Engineering*, vol. 8, no. 6, 2010.

[11] H. F. Taylor, "Proposed structure for calcium silicate hydrate gel," *Journal of the American Ceramic Society*, vol. 69, no. 6, pp. 464-467, 1986.

[12] J. M. Makar and G. W. Chan, "Growth of Cement Hydration Products on Single-Walled Carbon Nanotubes," *Journal of the American Ceramic Society*, vol. 92, no. 6, pp. 1303-1310, 2009.

[13] I. Richardson and G. Groves, "Models for the composition and structure of calcium silicate hydrate (C・S・H) gel in hardened tricalcium silicate pastes," *cement and concrete research*, vol. 22, no. 6, pp. 1001-1010, 1992.

[14] I. Richardson, "Tobermorite/jennite-and tobermorite/calcium hydroxide-based models for the structure of CSH: applicability to hardened pastes of tricalcium silicate, β-dicalcium silicate, Portland cement, and blends of Portland cement with blast-furnace slag, metakaolin, or silica fume," *Cement and Concrete Research,* vol. 34, no. 9, pp. 1733-1777, 2004.

[15] J. Moon, S. Yoon, and P. J. Monteiro, "Mechanical properties of jennite: A theoretical and experimental study," *Cement and Concrete Research,* vol. 71, pp. 106-114, 2015.

[16] S. Hamid, "The crystal structure of the 11 Ä natural tobermorite Ca2. 25 [Si3O7. 5 (OH) 1.5]· 1H2O," *Zeitschrift für Kristallographie-Crystalline Materials,* vol. 154, no. 1-4, pp. 189-198, 1981.

[17] P. Rejmak, J. S. Dolado, M. J. Stott, and A. s. Ayuela, "29Si NMR in cement: a theoretical study on calcium silicate hydrates," *The Journal of Physical Chemistry C,* vol. 116, no. 17, pp. 9755-9761, 2012.

[18] R. P. Selvam, V. J. Subramani, S. Murray, and K. D. Hall, "Potential application of nanotechnology on cement based materials," 2009.

[19] H. F. Taylor, *Cement chemistry*. Thomas Telford, 1997.

[20] R. J.-M. Pellenq *et al.*, "A realistic molecular model of cement hydrates," *Proceedings of the National Academy of Sciences,* vol. 106, no. 38, pp. 16102-16107, 2009.

[21] A. J. Allen, J. J. Thomas, and H. M. Jennings, "Composition and density of nanoscale calcium–silicate–hydrate in cement," *Nature materials,* vol. 6, no. 4, pp. 311-316, 2007.

[22] I. G. Richardson, "Model structures for C-(A)-SH (I)," *Acta Crystallographica Section B: Structural Science, Crystal Engineering and Materials,* vol. 70, no. 6, pp. 903-923, 2014.

[23] A. Al-Ostaz, W. Wu, A.-D. Cheng, and C. Song, "A molecular dynamics and microporomechanics study on the mechanical properties of major constituents of hydrated cement," *Composites Part B: Engineering,* vol. 41, no. 7, pp. 543-549, 2010.

[24] D. Hou, Y. Zhu, Y. Lu, and Z. Li, "Mechanical properties of calcium silicate hydrate (C–S–H) at nano-scale: a molecular dynamics study," *Materials Chemistry and Physics,* vol. 146, no. 3, pp. 503-511, 2014.

[25] Y. Janik, W. Kurdowski, R. Podsiadly, and J. Samseth, "Fractal structure of CSH and tobermorite phases," *ACTA PHYSICA POLONICA SERIES A,* vol. 100, no. 4, pp. 529-538, 2001.

[26] R. T. Cygan, J.-J. Liang, and A. G. Kalinichev, "Molecular models of hydroxide, oxyhydroxide, and clay phases and the development of a general force field," *The Journal of Physical Chemistry B,* vol. 108, no. 4, pp. 1255-1266, 2004.

[27] D. Hou, T. Zhao, P. Wang, Z. Li, and J. Zhang, "Molecular dynamics study on the mode I fracture of calcium silicate hydrate under tensile loading," *Engineering Fracture Mechanics,* vol. 131, pp. 557-569, 2014.
[28] M. Bauchy, H. Laubie, M. A. Qomi, C. Hoover, F.-J. Ulm, and R.-M. Pellenq, "Fracture toughness of calcium–silicate–hydrate from molecular dynamics simulations," *Journal of Non-Crystalline Solids,* vol. 419, pp. 58-64, 2015.
[29] H. M. Jennings, "A model for the microstructure of calcium silicate hydrate in cement paste," *Cement and concrete research,* vol. 30, no. 1, pp. 101-116, 2000.
[30] H. M. Jennings, "Refinements to colloid model of CSH in cement: CM-II," *Cement and Concrete Research,* vol. 38, no. 3, pp. 275-289, 2008.
[31] R. Feldman and P. Sereda, "A new model for hydrated Portland cement and its practical implications," *Engineering Journal,* vol. 53, no. 8-9, pp. 53-59, 1970.
[32] S. Merlino, E. Bonaccorsi, and T. Armbruster, "The real structures of clinotobermorite and tobermorite 9 Å: OD character, polytypes, and structural relationships," *European Journal of Mineralogy,* pp. 411-429, 2000.
[33] S. Plimpton, "Fast parallel algorithms for short-range molecular dynamics," *Journal of computational physics,* vol. 117, no. 1, pp. 1-19, 1995.
[34] H. Manzano, S. Moeini, F. Marinelli, A. C. Van Duin, F.-J. Ulm, and R. J.-M. Pellenq, "Confined water dissociation in microporous defective silicates: mechanism, dipole distribution, and impact on substrate properties," *Journal of the American Chemical Society,* vol. 134, no. 4, pp. 2208-2215, 2012.
[35] D. Hou, Z. Li, and T. Zhao, "Reactive force field simulation on polymerization and hydrolytic reactions in calcium aluminate silicate hydrate (C–A–S–H) gel: structure, dynamics and mechanical properties," *RSC Advances,* vol. 5, no. 1, pp. 448-461, 2015.
[36] K. D. Nielson, A. C. van Duin, J. Oxgaard, W.-Q. Deng, and W. A. Goddard, "Development of the ReaxFF reactive force field for describing transition metal catalyzed reactions, with application to the initial stages of the catalytic formation of carbon nanotubes," *The Journal of Physical Chemistry A,* vol. 109, no. 3, pp. 493-499, 2005.
[37] R. F. Feldman, "Factors affecting Young's modulus—porosity relation of hydrated Portland cement compacts," *Cement and Concrete Research,* vol. 2, no. 4, pp. 375-386, 1972.
[38] H. Manzano, J. Dolado, and A. Ayuela, "Elastic properties of the main species present in Portland cement pastes," *Acta Materialia,* vol. 57, no. 5, pp. 1666-1674, 2009.
[39] D. Hou, H. Ma, Y. Zhu, and Z. Li, "Calcium silicate hydrate from dry to saturated state: structure, dynamics and mechanical properties," *Acta materialia,* vol. 67, pp. 81-94, 2014.

[40] H. Suzuki, S. Bae, and M. Kanematsu, "Nanostructural deformation analysis of calcium silicate hydrate in portland cement paste by atomic pair distribution function," *Advances in Materials Science and Engineering*, vol. 2016, 2016.

[41] H. Manzano, A. K. Mohamed, R. K. Mishra, and P. Bowen, "A discussion on the paper “Role of porosity on the stiffness and stability of (001) surface of the nanogranular C–S–H gel”," *Cement and Concrete Research*, vol. 102, pp. 227-230, 2017.

[42] J. Gao, W. Luedtke, D. Gourdon, M. Ruths, J. Israelachvili, and U. Landman, "Frictional forces and Amontons' law: from the molecular to the macroscopic scale," ed: ACS Publications, 2004.

**List of Tables**

519 Table 1 Characteristics of the five models used in the simulation

| Model Name | Original structures from Richardson [22] | Supercell unit (Å× Å×Å) | Crystalline Structure | Mean length of silicate chain | Bridging tetrahedral connection |
|---|---|---|---|---|---|
| Model I | T2_ac | 45.4×43.8×43, β = 98.4° | monoclinic | 2 Å | adjacent |
| Model II | T2_ac | 45.4×43.8×43 | orthorhombic | 2 Å | adjacent |
| Model III | T11_14sc | 45.4×43.8×52.7, β = 95.5° | monoclinic | 11 Å | staggered |
| Model IV | T11_14sc | 45.4×43.8×52.7 | orthorhombic | 11 Å | staggered |
| Model V | T11_14sc | 45.4×43.8×52.7 | orthorhombic | 11 Å | staggered |

520

521 Table 2 Simulated results for the mechanical properties of C-S-H nanostructures
522 along y- and z- directions

| | Modulus of Elasticity in y-direction (GPa) | Strength in y-direction (GPa) | Modulus of Elasticity in z-direction (GPa) | Strength in z-direction (GPa) |
|---|---|---|---|---|
| Model I | 85.53 | 9.13 | 46.97 | 7.44 |
| Model II | 87.22 | 8.95 | 44.88 | 7.15 |
| Model III | 108.10 | 11.78 | 53.42 | 1.93 |
| Model IV | 112.71 | 11.17 | 51.29 | 1.92 |
| Model V | 116.8 | 10.94 | 38.39 | 1.15 |

523

524 Table 3 Simulated results for the mechanical properties of the C-S-H interfaces along
525 x-, y- and z- directions, and W0, W5, W10, W15, W20 stand for the interface with a
526 water layer of 0.0, 0.5, 1.0, 1.5, 2.0 Å added, respectively.

527

| [001] | W0 | W5 | W10 | W15 | W20 |
|---|---|---|---|---|---|
| Maximum Stress (GPa) | 1.64 | 1.04 | 0.98 | 0.85 | 1.05 |
| Young's modulus (GPa) | 49.41 | 34.65 | 27.14 | 27.25 | 30.65 |
| Fracture energy ($J/m^2$) | 1.20 | 0.50 | 0.59 | 0.29 | 0.50 |
| [010] | | | | | |
| Maximum Stress (GPa) | 13.42 | 5.29 | 1.93 | 1.27 | 1.33 |
| Young's modulus (GPa) | 102.18 | 44.25 | 19.15 | 12.29 | 11.49 |
| Fracture energy ($J/m^2$) | 5.51 | 1.80 | 0.34 | 0.36 | 0.31 |
| [100] | | | | | |
| Maximum Stress (GPa) | 6.09 | 3.05 | 1.88 | 1.45 | 1.14 |
| Young's modulus (GPa) | 75.79 | 53.28 | 34.06 | 25.87 | 15.48 |
| Fracture energy ($J/m^2$) | 3.79 | 0.91 | 0.76 | 0.43 | 0.32 |

528

**List of Figures**

543

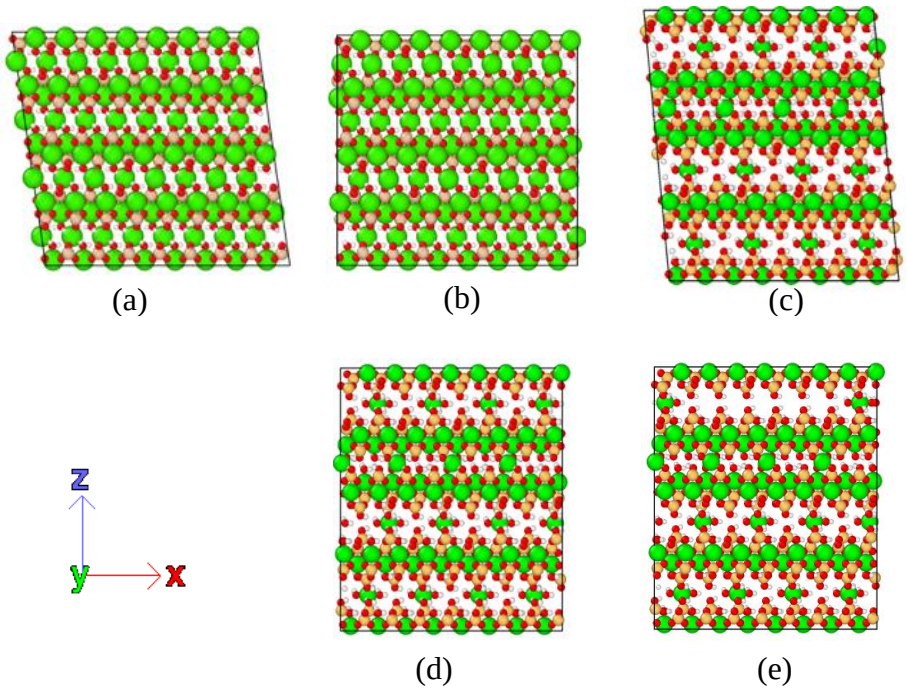


Figure 1 Molecular structures of (a) Model I, (010) surface of T2_ac in monoclinic structure (b) Model II, (010) surface of T2_ac in orthorhombic structure (c) Model II, (010) surface of T11_14sc in monoclinic structure (d) Model IV, (010) surface of T11_14sc in orthorhombic structure (e) Model V, (010) surface of T11_14sc with IGP in orthorhombic structure. Green atoms are Calcium, cantaloupe atoms are Silicon, red atoms are Oxygen and white atoms are Hydrogen in water molecules.

544
545

546
547

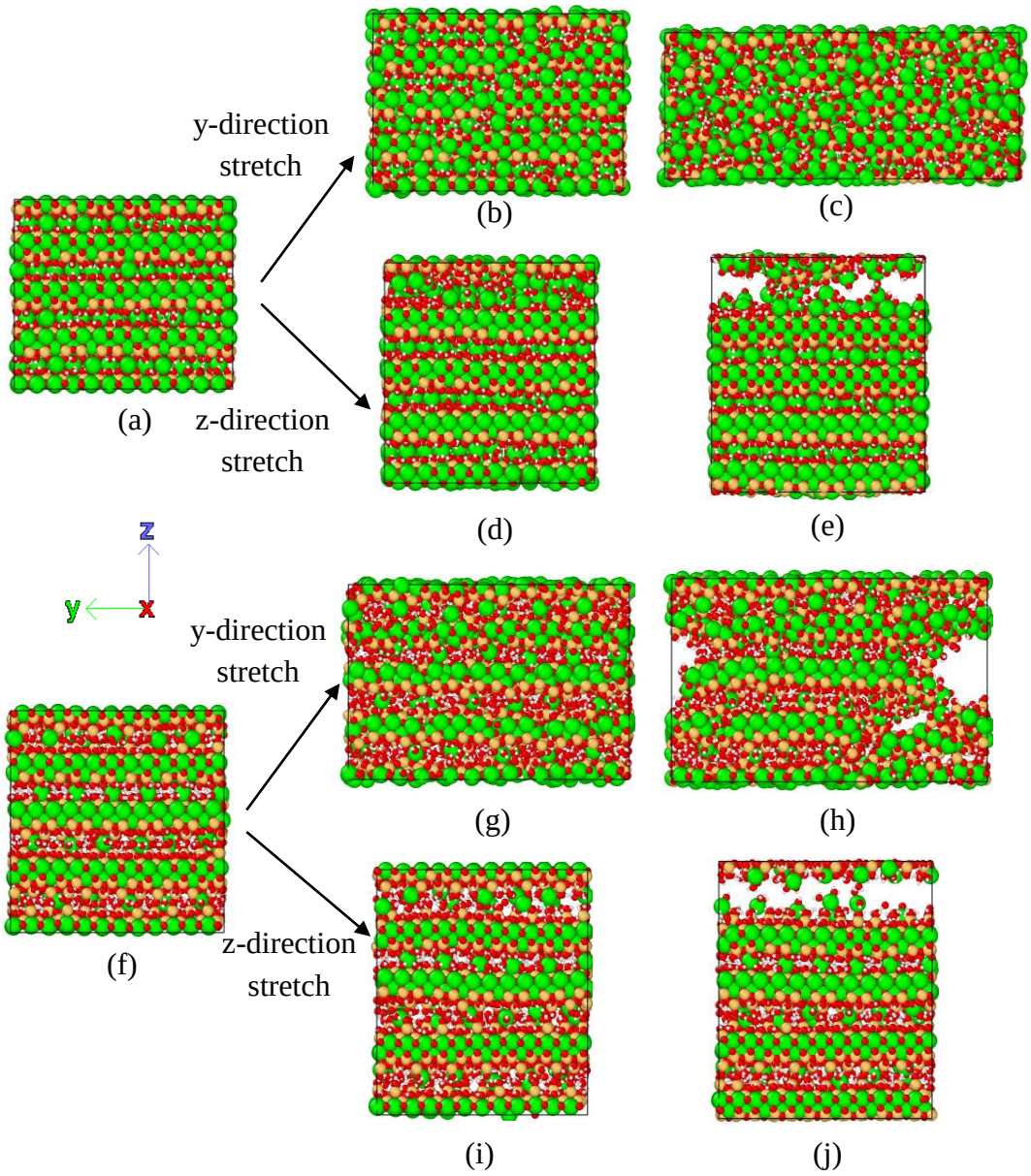


Figure 2 Tensile test simulation of Model I and Model III along z- and y- Directions. (a) Model I after equilibrium. (b) After the maximum value of the stress for Model I along y-direction. (c) The failure happens in Model I along y-direction. (d) After the maximum value of the stress for Model I along z-direction. (e) The failure happens in Model I along z-direction. (f) Model III after equilibrium. (g) Model III after the maximum value of the stress along y-direction. (h) The failure happens in Model I along y-direction, (i) After the maximum value of the stress for Model I in z-direction. (j) The failure happens in Model I along z-direction.

548

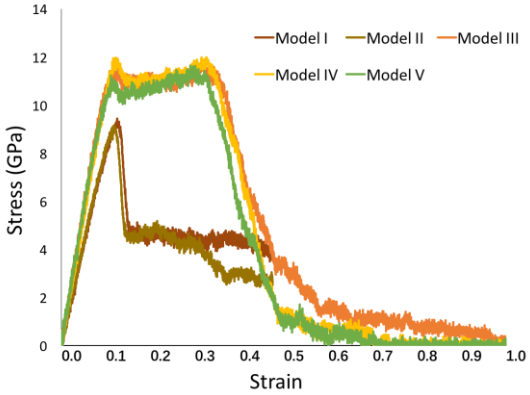


(a)

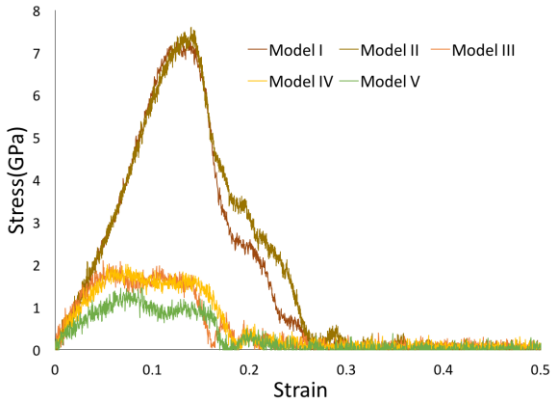


(b)

Figure 3 Stress-strain curves for five different C-S-H structrues along (a) y-direction (b) z-direction

549

550

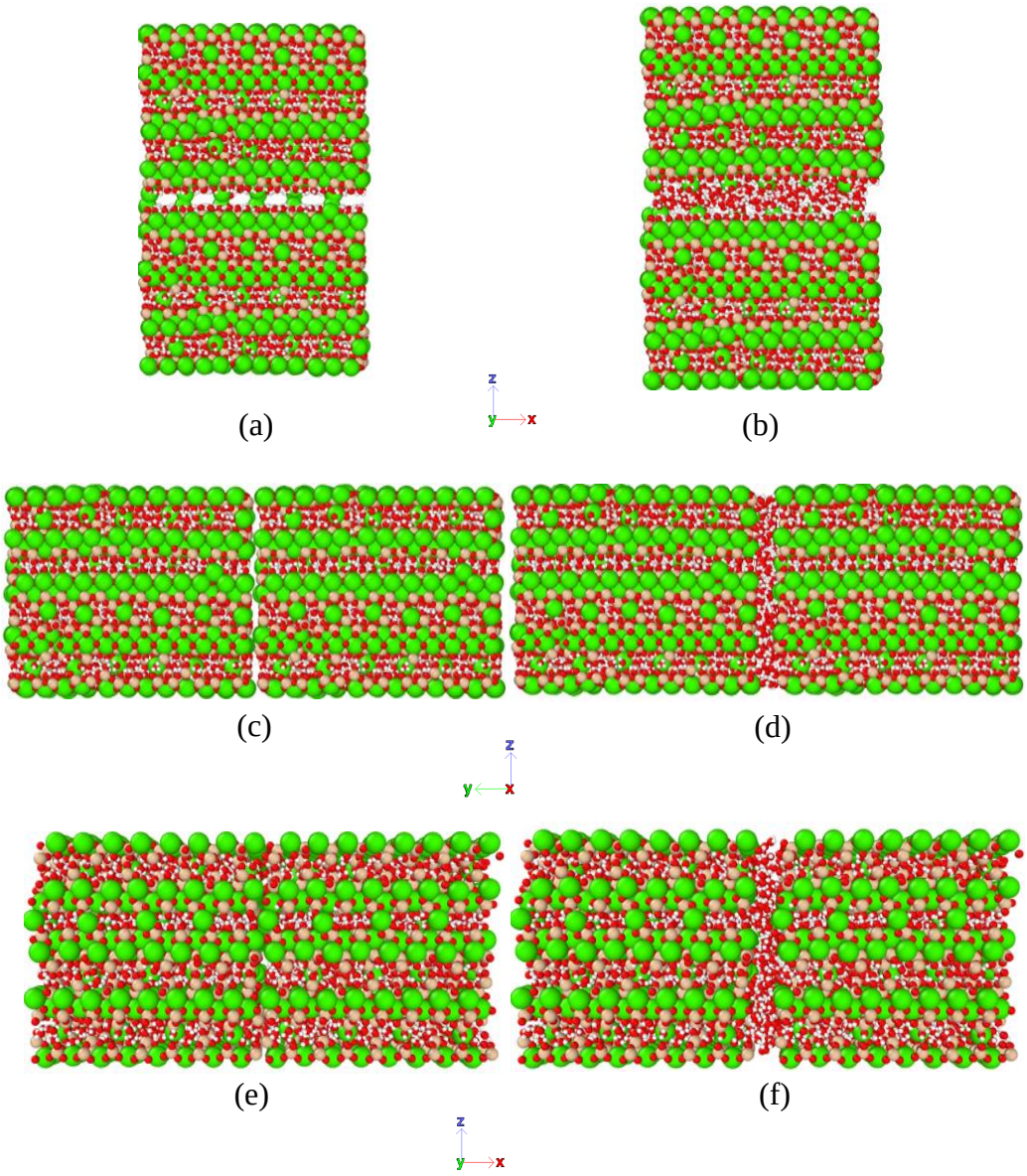


Figure 4 Molecular structure of (a) (001) surface with 0 Å water layer (b) (001) surface with 2.0 Å water layer (c) (010) surface with 0 Å water layer (d) (010) surface with 2.0 Å water layer (e) (100) surface with 0 Å water layer (f) (100) surface with 2.0 Å water layer

551

552

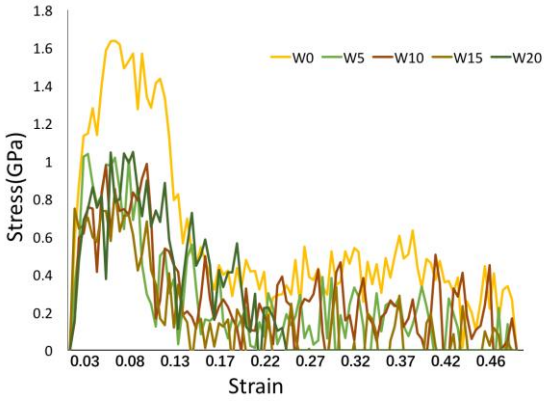


(a)

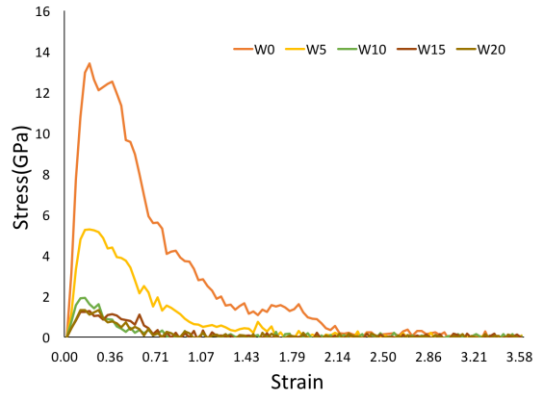


(b)

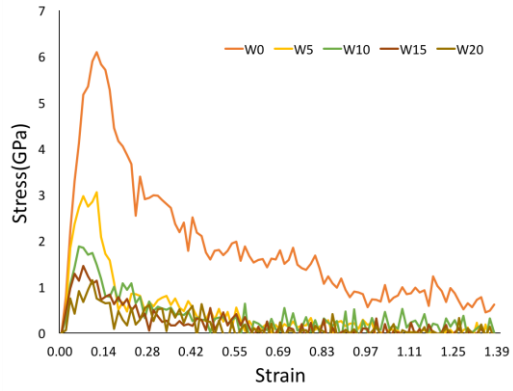


(c)

Figure 5 Tensile stress-strain curve for different water content in (a) (001) interface (b) (010) interface (c) (100) interface. W0, W5, W10, W15, W20 stand for the interface with a water layer of 0.0, 0.5, 1.0, 1.5, 2.0 Å added, respectively.

553

554

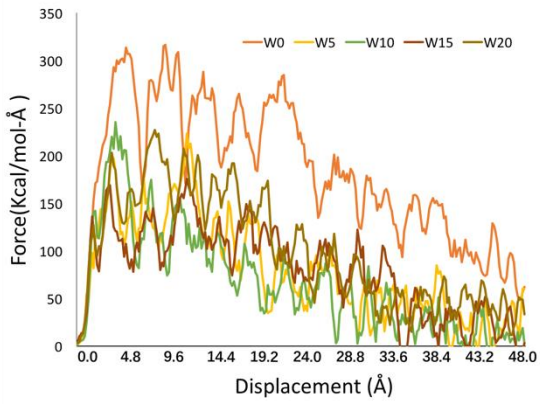


(a)

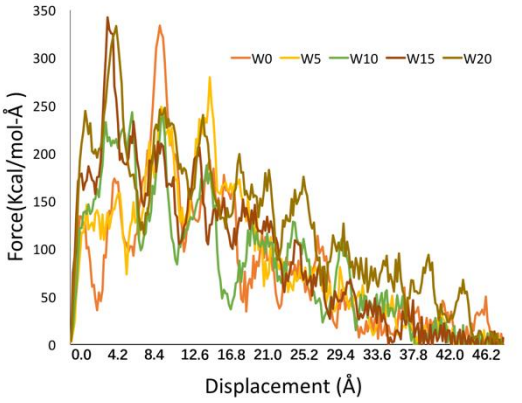


(b)

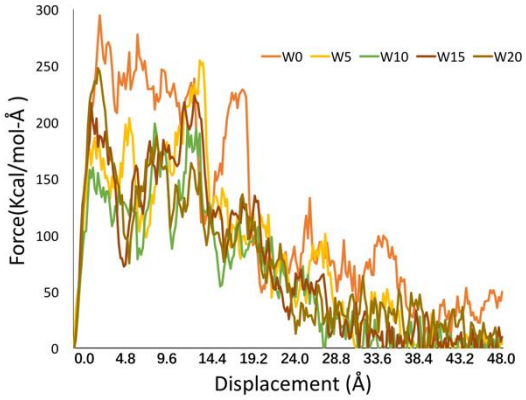


(c)

Figure 6 Shear force-displacement curve for different water content in (a) (001) interface (b) (010) interface (c) (100) interface

555

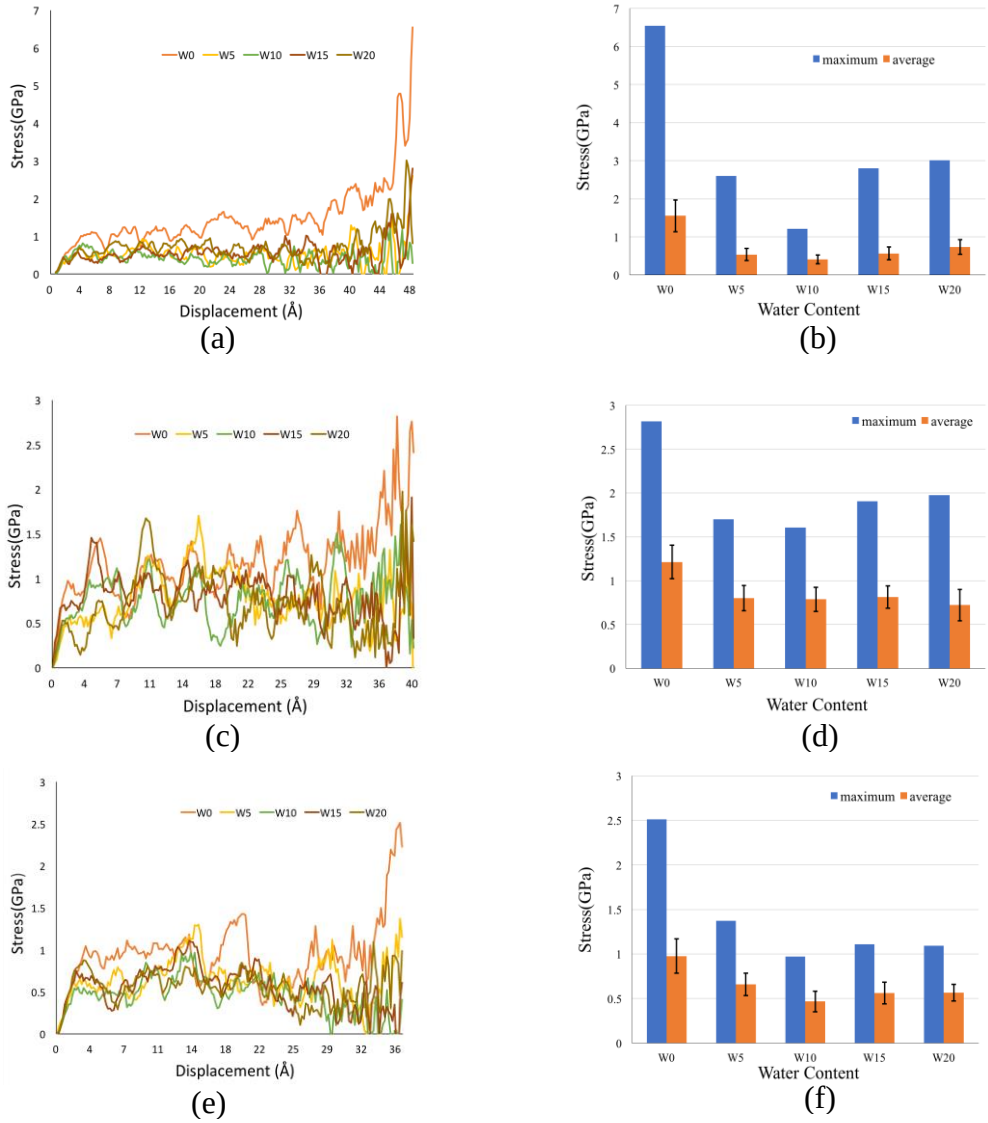


Figure 7 Stress-displacement curve for different water content in (a) (001) interface (c) (010) interface (e) (100) interface. Maximum value and average value of stress for each curve in (b) (001) interface (d) (010) interface (f) (100) interface.

556

557